12-2022

DFT Investigation of Lewis Acid Assisted C-CN Bond Activation of Benzonitrile with [Ni(dmpe)] Fragment

Lubna Kader
The University of Texas Rio Grande Valley

DFT INVESTIGATION OF LEWIS ACID ASSISTED C-CN BOND ACTIVATION OF BENZONITRILE WITH [NI(DMPE)] FRAGMENT

A Thesis

by

LUBNA KADER

Submitted in Partial Fulfillment of the

Requirements for the Degree of

MASTER OF SCIENCE

Major Subject: Chemistry

The University of Texas Rio Grande Valley

December 2022

DFT INVESTIGATION OF LEWIS ACID ASSISTED C-CN BOND ACTIVATION OF BENZONITRILE WITH [NI(DMPE)] FRAGMENT

A Thesis
by
LUBNA KADER

COMMITTEE MEMBERS

Dr. Tülay A. Ateşin
Chair of Committee

Dr. William D. Jones
Committee Member

Dr. Manar Shoshani
Committee Member

Dr. Evangelia Kotsikorou
Committee Member

December 2022

ABSTRACT

Kader, Lubna, DFT Investigation of Lewis Acid Assisted C-CN Bond Activation of Benzonitrile with [Ni(dmpe)] Fragment. Master of Science (MS), December, 2022, 45 pp., 5 tables, 15 figures, references, 45 titles.

There has been recent interest in the field of organometallics with C—C bond activation of organic substrates that are mediated by transition metal complexes. The bond activation of C—C bonds is important, not only in organic synthesis but also in industrial processes. However, the activation of these bonds remains difficult since they are thermodynamically more stable and sterically less available to activate than the activation of the C—H bond. Most of the successful C—C cleavage uses the relief of ring strain, achievement of aromaticity, or proximity, as the driving force for the reaction.[3] Another strategy is the use of a functional group such as nitrile and Lewis acid additivities. The studies looking at the mechanisms of C—C cleavage can be useful to develop new strategies for breaking C—C bonds. For this project, we compared the C—C bond activation transition state (TS) with and without Lewis acid coordination. There are two distinct TS structures found in the potential energy surface (PES) of C—C bond activation of benzonitrile without a Lewis acid, whereas there is only one TS structure on the PES with a Lewis acid. This suggests a post-transition state bifurcation for the Lewis acid assisted C—C bond activation with the [Ni(dmpe)] fragment. The structure of the C—CN bond activation products of benzonitrile with and without Lewis acid coordination are also reported.

DEDICATION

First, I would like to dedicate this thesis to my loving parents, Abdul Kader and Kazi Khaleda. Without their support, I would not have been able to focus so heavily on my studies as I did. Secondly, I would also like to thank my only sister Anika Kader, for providing laughter and peace in a time of great stress in my life. Finally, I would like to dedicate this work to my husband Firoz Ahmed who has been stuck by my side since the beginning of my journey as a new student in Chemistry. Through his love, comfort, and reliability, I was able to focus on my goal successfully. Finally, I would like to thank my friend Tanjida Tuba for her kind support and inspiration. Thank you all for pushing me to always do my best and for continuously believing in me. I cannot put into words the love and gratitude I feel for you.

ACKNOWLEDGMENTS

I would like to acknowledge my advisor, my mentor, and thesis committee chair, Dr. Tülay Ateşin, for always providing great guidance and accepting me as her research student. She placed her confidence in me and believed I would always reach my goal, without her then I'm not confident that I would have accomplished as much as I did. I would also like to thank Dr. Abdurrahman Ateşin, I would not have known as much as I do about computer software without him. Additionally, a big thank you to Dr. William Jones for providing additional guidance. It was a great honor to work with him and this important opportunity allowed me to grow as a chemist and become more confident in my work as an organometallic chemist. I would like to thank my committee members Dr. Manar Shoshani and Dr. Evangelia Kotsikorou for their time and expertise. Finally, I would like to thank the University of Texas Rio Grande Valley and the Chemistry Department for providing me with a great experience as a graduate student.

TABLE OF CONTENTS

Page

LIST OF TABLES

LIST OF FIGURES

CHAPTER I

INTRODUCTION

C-C Bond Activation

The activation of carbon—carbon σ-bonds (C—C) has many important applications in both organic synthesis and industrial processes. Researchers are becoming more and more interested in the C—C bond activation due to its wide range of uses. Over the past few decades, research into the C—C bond activation in organic substrates via transition metal complexes in homogeneous systems has grown significantly (Pettersen et al., 2004). Converting a C—C single bond into two transition M—C bonds often entails the oxidative addition of a low valent transition metal complex as shown in **Figure 1** (Laird et al., 1996). Alkanes, for instance, can undergo skeletal rearrangement or cracking when the C—C link is broken, which is crucial for the industrial refining of petroleum. In organic synthesis, the transition metal-catalyzed activation of C—C bond has been exploited, and the advantages of atom economy and chemo selectivity have been highlighted (Martinez et al., 2017).

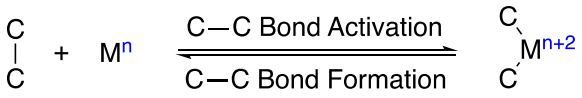

Figure 1: C–C bond activation by a metal (oxidative addition) and C–C bond formation by a metal (reductive elimination)

Organometallic chemistry faces a significant barrier since the target C—C bond is both strong and kinetically inert, making its breakage under mild homogenous circumstances difficult. It has been established that a variety of techniques favor C—C bond cleavage with transition metal complexes. The activation is mainly restricted to systems where achieving aromatization or relief of ring strain function as a driving force (Taw et al., 2002), or close proximity of the metal center to the C—C bond. Recent developments have shown an increasing number of organometallic reagents have successfully performed this activation via the insertion of a transition-metal center into the C—C bond. One area of recently increased study is the C—C bond activation of alkyl and aryl nitrile substrates (Peverati & Truhlar, 2012), Biphenylene, C—C≡C bonds, C—CN bonds, and aryl—CH_3 bonds are some of the systems where mechanistic knowledge about the C—C cleavage has been discovered (Clot et al., 2003).

Why Ni is used

The chemical element nickel has the atomic number 28 and the symbol Ni. To fully comprehend the significance of nickel, it is crucial to compare all the Group 10 metal's reactivity and traits. First, let's talk about electronegativity (EN), which Pauling described in 1932 as an atom or molecule's propensity to draw electrons to itself based on factors like its atomic number (Properties et al., 1985). This is well illustrated by the lanthanoid contraction, where Dongfeng Xue shows that the transition metals in the third row have somewhat higher values than those in the second row. It was also mentioned that the longer relativistic effects are what cause these higher

EN levels. Dongfeng Xue also demonstrates how the complexes of Mn^{2+} and Zn^{2+} boost the stability of a divalent metal ($M^{2+)}$ ion (K. Li & Xue, 2006).

Additionally, it has been demonstrated that nickel can activate C—C bonds through a variety of organometallic processes. Pd and Pt, which are both more stable metals than nickel, have been proven to undergo reductive elimination more easily, while nickel, due to its oxophilicity, easilyconducts oxidative addition (Forlemu et al., 2017). It is also noteworthy that while palladium and platinum easily eliminate β-hydrides, nickel also undergoes β-migratory insertion. According to Valentine Ananikov, the homolytic M—C bond cleavage trend is as follows: Ni—C > Pd—C > Pt—C. It was also noted that the M—C bond strength increases in the following order: Ni—C, Pd—C, Pt—C. Even though palladium and platinum are quite like nickel, Pd has been used and modified for a variety of chemistry purposes (Nakazawa et al., 2005).

C—CN Bond Activation

Since it was first reported in the 1970s, C—CN bond activation has drawn attention. The stable C—C bond's lack of reactivity makes it difficult for the less stable M—C bonds to form, which is mainly caused by its kinetic inaccessibility and thermodynamic stability. Despite being inconvenient, ways to get around these obstacles have been put forth and put into practice (Garcia et al., 2002). With the help of numerous transition metal complexes, it has been possible to achieve C—CN bond activation despite the comparatively high bond dissociation energy caused by the cyano group's distinctive properties (such as electron-withdrawing, polarized bonds, and high

affinity for specific metals) (Nakao et al., 2006). Traditionally, C—CN bonds were cleaved using metals such as Fe and Rh in tactical combination with organic silicon reagents or metal–Lewis acid bifunctional catalysts (**Figure 2**) (Souillart & Cramer, 2015). Most recently, Ni(0) and Pd(0) mediated C—CN bonds cleavage were reported. The first systematic study of the cleavage of the C—CN bond was initiated in the 60s by Bergman and co-workers who described the C—CN bond disconnection reaction (Nakao et al., 2006).

Because of their high bond dissociation energies, C—CN bonds typically endure the different reaction conditions of numerous organic transformations (T. Li et al., 2010). But low-valent transition metal complexes have demonstrated that nitriles' C—CN bonds can be broken. Nitriles can either coordinate in a η^1 or η^2 way to a metal center. Low-valent metal complexes frequently exhibit η^2 coordination, which can be reinforced through π-back donation, whereas high-valent Lewis acidic metal complexes promote η^1 coordination of the nitrogen atom in nitriles (Taw et al., 2002).

The activation of C—CN bonds is frequently started by η^2-coordination. The production of silylisonitrile complexes and oxidative addition have been identified as the two primary routes for the cleavage stage. When a team from DuPont explained how benzonitrile adds to nickel (0) species at room temperature in 1971, oxidative addition had already been documented (**Figure 3**) (Nakazawa et al., 2005).

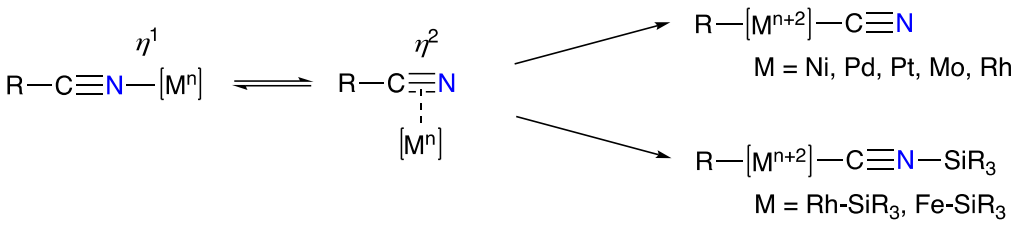

Figure 2: Two common pathways for the C—CN bond activation.

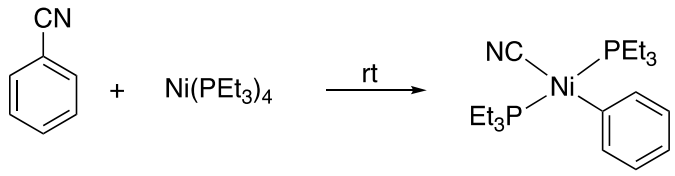

Figure 3: C—CN bond activation by Ni (PEt3)4

CHAPTER II

BACKGROUND

Role of Lewis acid

In the industrial setting, Lewis acids have been used with transition-metal catalysts to enhance product selectivity, accelerate reactions, and lengthen catalyst lifetimes. When Lewis acids were used to catalyze the hydrocyanation of olefins using Ni (0)-phosphite catalysts, for instance, it was discovered that the coordination of the Lewis acid through the nitrogen lone electron pair occurred before the reaction (Nakazawa et al., 2005). In palladium-phosphine complexes, Lewis acids have also been found to speed up reductive elimination. According to previous theories, this happened as a result of a shift in the charge distribution of the nitrogen, boron, or aluminum following Lewis acid coordination (Garcia et al., 2002). The resulting complex makes the nitrile carbon more vulnerable to nucleophilic attack by the alkyl group, boosting the pace of reaction, in this case reductive elimination (Nakao et al., 2006). The rate of reductive elimination in palladium-phosphine complexes was also demonstrated to be accelerated by Lewis acids. The pace of reaction, in this case reductive elimination, is accelerated because the resulting complex is more vulnerable to the alkyl group's nucleophilic attack on nitrile carbon.

Using [M(dippe)] fragement and a primary focus on group 10 metals, the Jones group experimented with the impact of Lewis acids on C—CN bond activation. For Ni and Pd, experimental data have been gathered, but not for platinum (García et al., 2004). The reaction rate of $[Ni(dippe)H]_2$ was greatly influenced by the Lewis acids BF_3 and BPh_3 in **Figure 4**. When less

than one equivalent is used, the reaction rate is 100 times higher, but when more than one equivalent is used, the reaction is suppressed (Swartz et al., 2011).

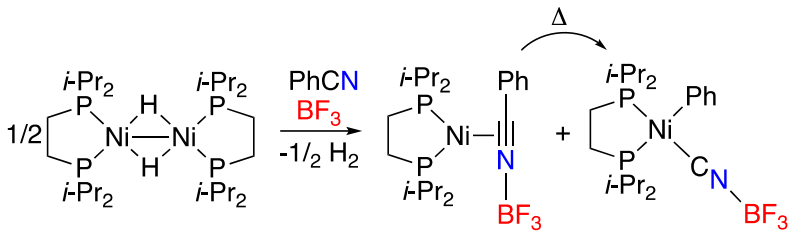

Figure 4: Lewis acid assisted C–CN bond activation of benzonitrile using the [Ni(dippe)] fragment.

For Pd, it was demonstrated that the Lewis acid connects to the nitrogen via coordinating with the nitrile's lone pair when it reacts with BEt_3 or BPh_3 in acetonitrile to generate the η^2 complex depicted in **Figure 5** (Munjanja et al., 2016). Through steric bulk or charge distribution on nitrogen or boron atoms, this coordination has been demonstrated to increase reaction rates, product selectivity, and can lengthen catalyst lifetime. The η^2 product can undergo C—CN bond cleavage under photochemical and thermal conditions to produce (dippe)Pd (Ph) (CN-BEt_3).

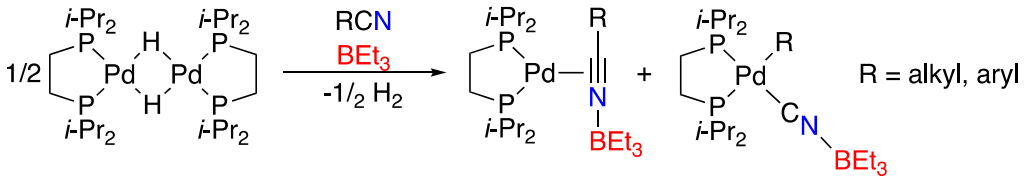

Figure 5: Lewis acid assisted C–CN bond activation of acetonitrile and benzonitrile by the [Pd(dippe)] fragment.

The $[Pt(dippe)H]_2$ in benzonitrile is the final reaction that will be covered. Platinum has been demonstrated to adhere to both C—C and C—H activation routes, with PtL_2 fragment favoring oxidative addition by C—H bond cleavage (Swartz et al., 2011). **Figure 6** depicts the reaction of $[Pt(dippe)H]_2$ in PhCN, with three of the products coming from the kinetically preferred C—H activation and one coming from the C—CN bond activation (Swartz et al., 2011).

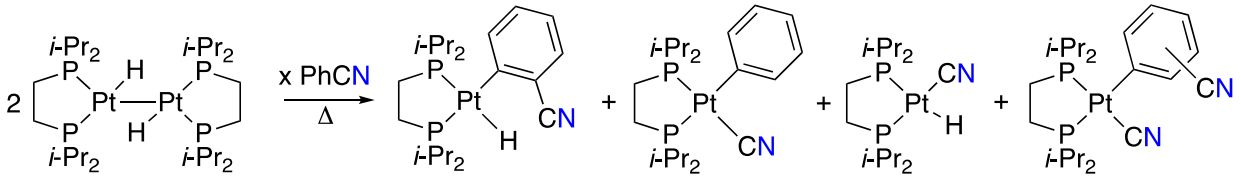

Figure 6: C–CN bond activation of benzonitrile with the [Pt(dippe)] fragment.

CHAPTER III

METHODOLOGY

Density Functional Theory

Density-functional theory (DFT) has developed into a crucial research tool for materials scientists, physicists, and chemists. In recent years, it has developed along two (quite independent) trajectories (Crabtree et al., 1985). The first one is about applying DFT to systems with many electrons. These techniques have grown significantly over the past ten years and are now successfully challenging conventional wavefunction-based approaches as the preferred method for doing large-scale quantum chemistry simulations (Lundberg & Siegbahn, 2005). Second, DFT has been very successful in developing theories for both fluids and phase transitions, two significant areas of statistical mechanics. With a few notable exceptions, applications in statistical mechanics have generally been classical, in contrast to the problem of electronic structure, which is fundamentally quantum mechanical in nature (Acosta-Ramírez et al., 2007).

Although statistical mechanical studies used to use but density-functional methods using modern functionals show very good accuracy for a wide range of applications (Lundberg & Siegbahn, 2005). The theorems of Hohenberg and Kohn are at the core of contemporary density-functional theory, which encompasses both quantum and classical systems (Becke, 1993). The selection of the external field totally determines the Hamiltonian and hence the ground-state wavefunction and energy for an *N*-particle system interacting with a specified interparticle interaction (r) (Brunkan et al., 2004). The ground state energy is therefore a function of (r) (Amusia et al.,

2003). The entire ground-state energy can be expressed as a function of ρ because Hohenberg and Kohn demonstrated in 1964 that there is a one-to-one correlation between the field (r) and the single-particle density ρ (r),

$E[\rho] = E_0 + E[\rho] + = \int d\mathbf{r}\, \boldsymbol{\phi}\,\mathbf{(r)}\, \rho\,\mathbf{(r)}$ …… (1)

Here $E_0[\rho]$ is a functional that is independent of the external potential, $\boldsymbol{\phi}\,\mathbf{(r)}$ is universal function for a given interparticle interaction (Becke, 2014).

Hohenberg and Kohn also proved a second theorem which provides an energy variational principle. They showed that for any trial density ρ(r) that satisfies $\int \rho\,(r)\, dr = N$

$E[\rho] > Eg$ ……. (2)

where Eg is the true ground-state energy. The equality in equation 2 holds only when ρ(r) is the true ground-state single-particle density (Yu et al., 2016).

Density-functional molecular-orbital theory has been used more frequently in settings like industrial research labs (Hopmann, 2016). The use of theoretical and computational chemistry in industry has a history dating back to the development of pharmaceutical research, and more recently, it has spread to a variety of other industrial sectors including automotive, chemicals, coatings, glass, materials, petroleum, and polymers (Zhao et al., 2012). The two main groups of theoretical techniques are classical and quantum mechanical. Traditional approaches, as employed in molecular dynamics and mechanics software, have been widely applied, for instance in the research of macromolecules in the pharmaceutical business. In more recent times, traditional

methods have been used in fields focused on materials, including polymers, catalysts, and zeolites (Swartz et al., 2011).

Computational Details

Density functional theory (DFT) calculations were performed on Lonestar6 supercomputers located at the University of Texas at Austin, Texas Advanced Computing Center. Previously published structures for the C—CN bond activation of the benzonitrile using [Ni(dmpe)] fragment was used as initial guess for the geometry optimizations. For this study, we modified the structures by adding Lewis acid coordinated to the nitrile (Martin & Buchwald, 2008). The structures were optimized in gas phase using redundant internal coordinates (Peng et al., 1996), and a wave function incorporating Becke's three-parameter hybrid functional (B3) (Becke, 1993), along with the Lee-Yang-Parr correlation functional (LYP) (Lecklider, 2011). Gaussian16 package was used for all calculations (Hugo et al., 2019). C, H, N, B and F were represented with 6-31G(d,p) (Hehre et al., 1972) basis sets and Ni and P atoms were represented with the effective core pseudopotentials of the Stuttgart group and the associated basis sets improved with a set of *f*-polarization functions for Ni (α = 3.130) (Ehlers et al., 1993) and a set of *d*-polarization functions for P (α = 0.387) (Ehlers et al., 1993). The geometry optimizations without any symmetry constraints were followed with frequency calculations to check whether the local minima have all positive frequencies and the transition states have only one negative frequency. The frequency calculations also were used to calculate the zero-point energies, thermal corrections and entropic corrections. The solvent effects were calculated using solvent model

density (SMD) (Höllwarth et al., 1993). The relative stability of the structures were evaluated by the free energies of solvation for the gas-phase optimized structures with 6-311++G(d,p) basis sets (Marenich et al., 2009) for C, H, N, B and F. The energies used throughout this thesis are the solvation corrected Gibbs free energies (at 298.15K and 1 atm) and calculated using the following equation:

$$G\ (\text{kcal/mol}) = (G(T) - E + SPE)\ x\ 627.5 \quad \text{..... (3)}$$

The *G(T)* is the "sum of electronic and thermal free energies", *E* is the "electronic energy" and *SPE* is "solvent corrected electronic energy." ChimeraX package was used to display the molecular structures (Krishnan et al., 1980).

CHAPTER IV

RESULTS AND DISCUSSION

As an initial guess for the C—CN bond activation transition state (TS) structure, we started our DFT analysis by adding the BF_3 to the already optimized structures with the [Ni(dmpe)] fragment. The C—CN bond activation TS search with the Lewis acid added failed from this initial guess. Therefore, we reinvestigated the potential energy surface (PES) with 1D scan along the C—CN interatomic distance to locate a better starting structure and also conducted a more detailed 2D PES scan around the C—CN bond activation TS with and without BF_3. **Figure 7** shows the optimized structure of the C—CN bond activation product starting from the X-ray single crystal structure.

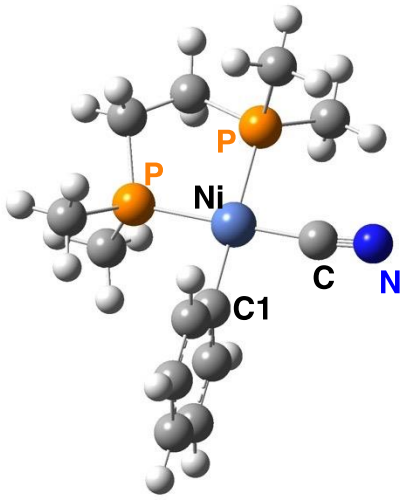

Figure 7: The C—CN bond activation product optimized from the X-ray single crystal structure.

TS can be localized in many cases through scanning one structural degree of freedom, in our case it is the C1—CN interatomic distance. This will only be successful if the reaction pathway can be described essentially with this structural parameter. To cover the relevant part of a PES, a series of calculations were performed in which the C1—CN interatomic distance was fixed to a certain value, while all other parameters were optimized. To locate the C—CN bond activation TS, a relaxed PES scan was performed automatically in redundant internal coordinate system by starting with the C1—CN interatomic distance of 2.65Å and decreasing it to 1.40 Å by a step size of 0.05 Å. The scan is shown in **Figure 8**. The energy increased as the C1—CN interatomic distance decreased from a larger distance (2.65 Å) until reaching a maximum at about 1.55 Å.

Further decreasing the C1—CN interatomic distance from 1.55Å to 1.50 Å led to a sudden decrease in energy suggesting a discontinuous or irregularly shaped PES. The optimized structure at 1.50 Å is an η^2-arene complex, which indicates the simultaneous rotation of the phenyl ring as the C1-CN interatomic distance decreases. Even though the structure at energy maximum looks like a reasonable TS, it is not clear whether this energy maximum corresponds to a true TS. To take into consideration the rotational TS, we performed 2D PES scan shown in **Figure 9**.

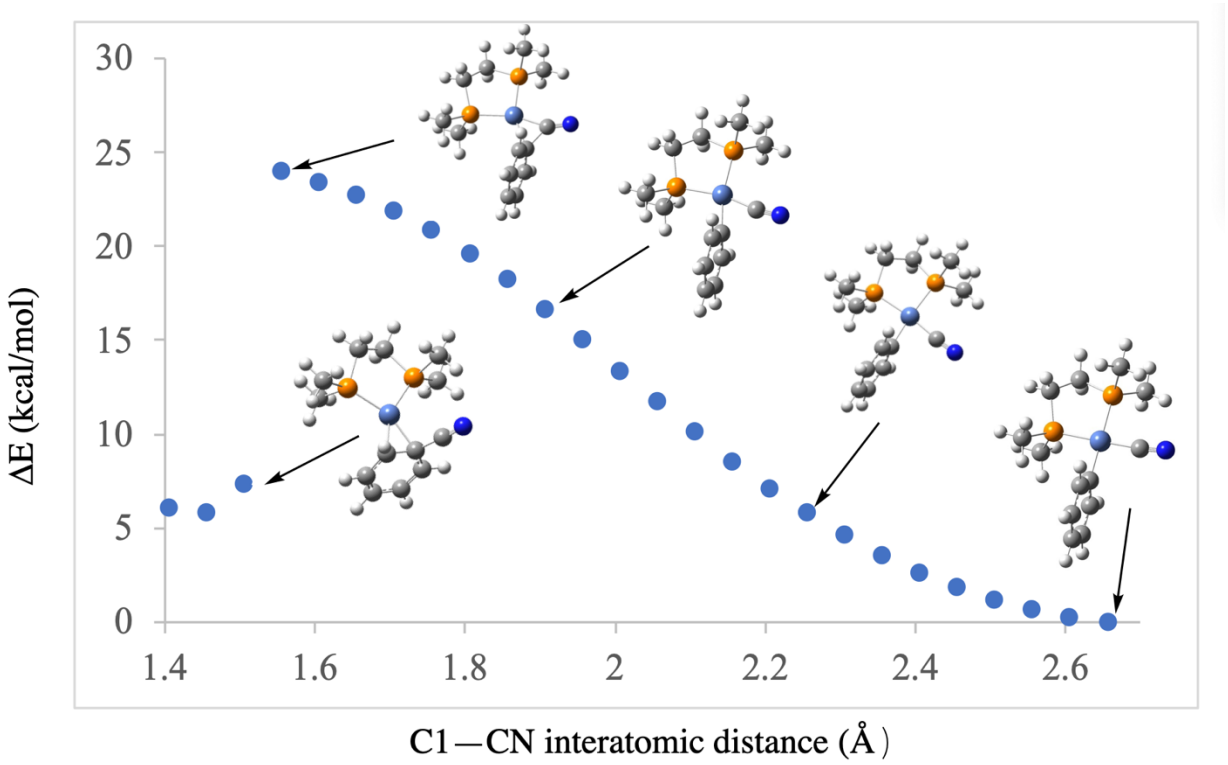

Figure 8: 1D PES scan to locate the C—CN bond activation TS.

In a 2D PES scan, we scanned the P-Ni-C1-C2 dihedral angle from -35.0° to -150.0° with a step size of 5.0° at the C1—CN interatomic distance of 1.55 Å, 1.60 Å, 1.65 Å, 1.70 Å and 1.75 Å. Although there seems to be a local maximum around -70.0° and 1.55 Å, there are two low energy saddle points on the PES which corresponds to two distant C—CN bond activation TS structures. These saddle points are marked with an arrow in **Figure 9**.

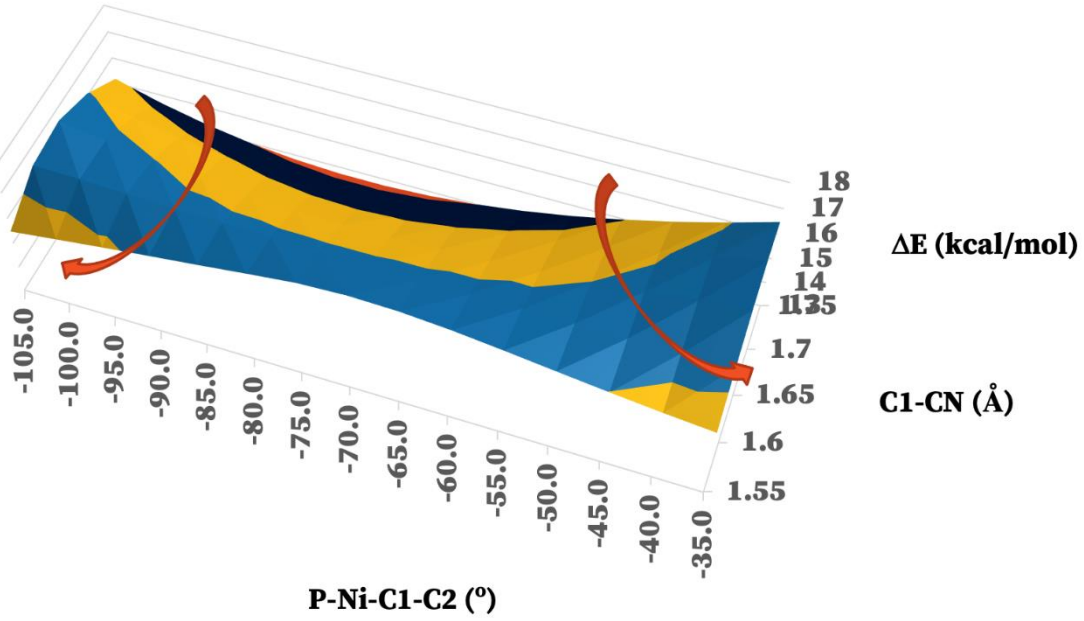

Figure 9: 2D PES scan to locate the C—CN bond activation TS. ΔE is reported in kcal/mol calculated by Gaussian16/C, H and N (6-31G**); Ni, P (SDDALL), αNi = 3.130, αP = 0.387.

Table 1 shows the data used to generate the 2D PES. The C1—CN interatomic distance is varied from 1.75 Å to 1.60 Å by a step size of 0.05 Å in one dimension. In the other dimension the P-Ni-C1-C2 dihedral angle was scanned from -35.0° to -105.0° by a step size of 5.0°.

Table 1: Potential energy surface scan to locate the C—CN bond activation TS. DE is reported in kcal/mol calculated by Gaussian16/C, H and N (6-31G**); Ni, P (SDDALL), a_{Ni} = 3.130, a_P = 0.387. Interatomic distances are in Å, and angles are in °.

	C1—CN			
P-NI-C1-C2	**1.75**	**1.7**	**1.65**	**1.6**
-35.0	16.4832777	16.7001439	16.6202204	16.2308022
-40.0	15.9229056	16.2924826	16.387221	16.19806
-45.0	15.4133229	15.9223666	16.1810218	16.18932
-50.0	14.9618483	15.5948528	16.0006723	16.1966443
-55.0	14.5711462	15.3114291	15.8436059	16.207184
-60.0	14.2462648	15.0753605	15.7132307	16.2120672
-65.0	13.9945159	14.8949074	15.6126057	16.2093106
-70.0	13.8213533	14.7755375	15.5507821	16.2047674
-75.0	13.7321559	14.7272637	15.5367485	16.2019097
-80.0	13.731005	14.7521991	15.5718037	16.2092955
-85.0	13.8201798	14.8528567	15.6634308	16.2278328
-90.0	14.003783	15.0350517	15.813274	16.2656528
-95.0	14.2928072	15.3056774	16.0219311	16.3209691
-100.0	14.6808343	15.654802	16.2809296	16.3754614
-105.0	15.1725448	16.0809584	16.5681547	16.4089115

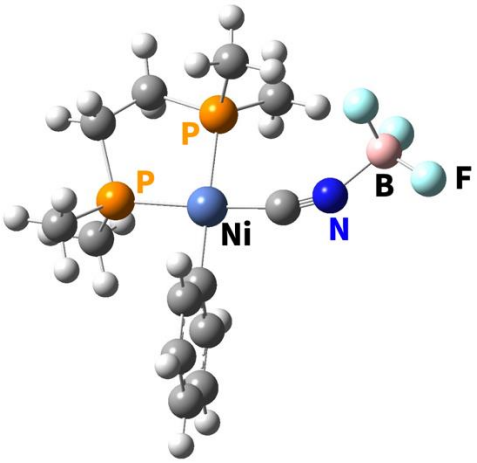

1-BF_3

Figure 10: The C—CN bond activation product with BF3 optimized from the X-ray single crystal structure.

To locate the Lewis acid-assisted C—CN bond activation TS, a relaxed PES scan was performed automatically in redundant internal coordinate system by starting with the C1—CN interatomic distance of 2.65Å and decreasing it to 1.40 Å by a step size of 0.05 Å starting from the C—CN bond activation product with BF_3 shown in **Figure 10**. The scan is shown in **Figure 11**.

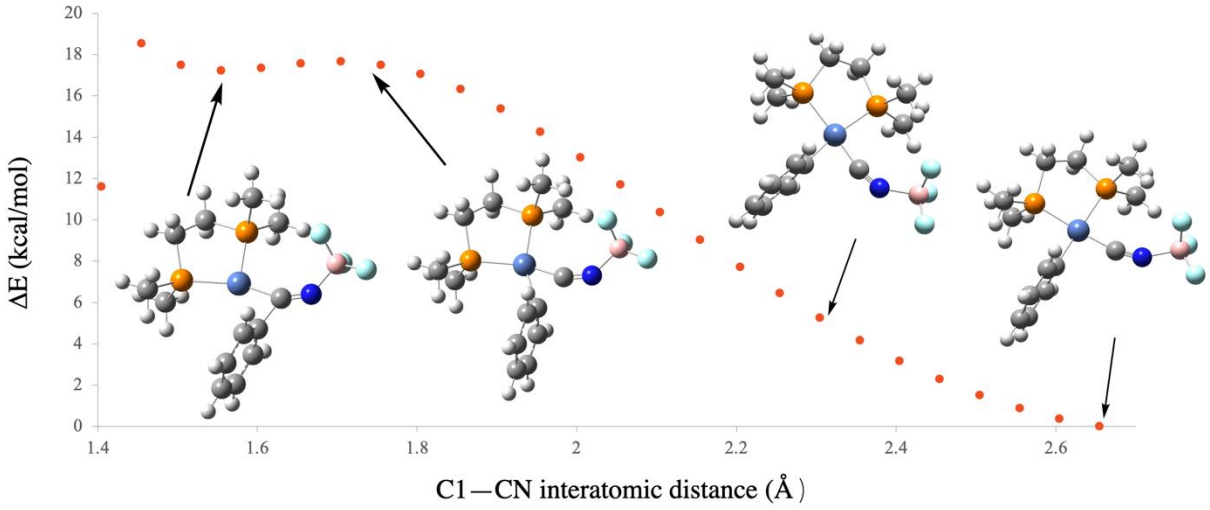

Figure 11: 1D PES scan to locate the Lewis acid assisted C—CN bond activation TS.

Contrary to the 1D scan without the Lewis acid, the energy increased as the C1—CN interatomic distance decreased from a larger distance (2.65 Å) until reaching a maximum at about 1.70 Å. Further decreasing the C1—CN interatomic distance led to a smooth decrease in energy suggesting a continuous or regular shaped PES. The optimized structure at 1.55 Å is an η^2-complex with C—CN bond. Further decreasing the C1-CN interatomic distance from 1.45 Å to 1.40 Å shows discontinuity. This 1D scan indicates the rotation of the phenyl ring occurs after the C—CN bond activation. To test this hypothesis, we performed 2D PES scan shown in **Figure 12**.

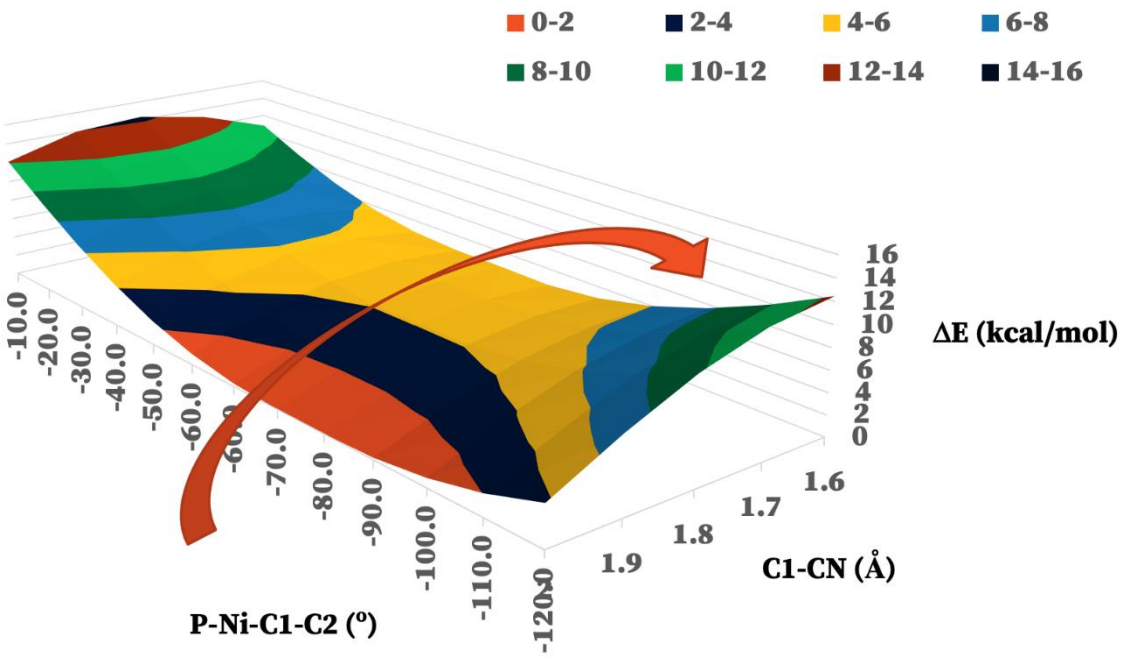

Figure 12: 2D PES scan to locate the Lewis acid assisted C—CN bond activation TS. ΔE is reported in kcal/mol calculated by Gaussian16/C, H, N, B and F (6-31G**); Ni, P (SDDALL), α_{Ni} = 3.130, α_{P} = 0.387.

In a 2D PES scan, we scanned the P-Ni-C1-C2 dihedral angle from -10.0° to -120.0° with a step size of 10.0° at the C1—CN interatomic distance of 1.6 Å, 1.7 Å, 1.8 Å, 1.9 Å and 2.0 Å. There is only one low energy saddle point on the PES which corresponds to one distinct C—CN bond activation TS structure with BF_3.

Table 2: Potential energy surface scan to locate the Lewis acid assisted C—CN bond activation transition state. DE is reported in kcal/mol calculated by Gaussian16/C, H, N, B and F (6-31G**); Ni, P (SDDALL), a_{Ni} = 3.130, a_P = 0.387. Interatomic distances are in Å, and angles are in degrees (°).

	C1—CN				
P-NI-C1-C2	**1.6**	**1.7**	**1.8**	**1.9**	**2.0**
-120.0	8.09895154	7.32279697	5.46355387	2.7016439	-0.5800389
-110.0	5.47403956	4.75751727	3.14954172	0.66928334	-2.3262674
-100.0	3.27699527	2.76552442	1.4275978	-0.77158	-3.5072601
-90.0	1.60373358	1.354085	0.30238452	-1.644139	-4.1720944
-80.0	0.50571658	0.53591237	-0.2541164	-1.9935616	-4.3559297
-70.0	0	0.28399848	-0.2745294	-1.9935616	-4.3559297
-60.0	0.08394829	0.28399848	-0.2745294	-1.8310114	-4.0754766
-60.0	0.08394829	0.53908757	0.22014933	-1.156457	-3.2993911
-50.0	0.39679967	1.23806468	1.22496855	0.05974523	-1.9885164
-40.0	1.23259907	2.42766049	2.75085324	1.80291781	-0.1367407
-30.0	2.58445014	4.11869954	4.76690482	4.03438102	2.15215222
-20.0	4.37954289	6.25633118	7.21105627	6.67245816	4.82630491
-10.0	6.47883995	8.73448112	9.98946974	9.60501319	7.74746436

The X-ray single crystal structures and optimized structures of the C—CN bond activation products are shown in Figure 13 and selected bond distances (Å) and angles (°) are summarized in **Table 3**. The phenyl ring is perpendicular to the P—Ni—P plane with a P—Ni—C—C1 dihedral angle of 88.68° for **1**, 91.61° for **1-BF$_3$** and 91.52° for **1-BPh$_3$**. The bond lengths did not show significant differences. The C—N bond lengths were all within 1.16-1.17 Å. The Ni—CN bond lengths are around 1.85-1.87 Å. The Ni—C_{aryl} bonds at within 1.92-1.94 Å. The N—B bond lengths is considerably shorter in **1-BF$_3$** compared to **1-BPh$_3$**. The C—N—B is more bent with 158° in **1-BF$_3$** compared to 173° in **1-BPh$_3$**.

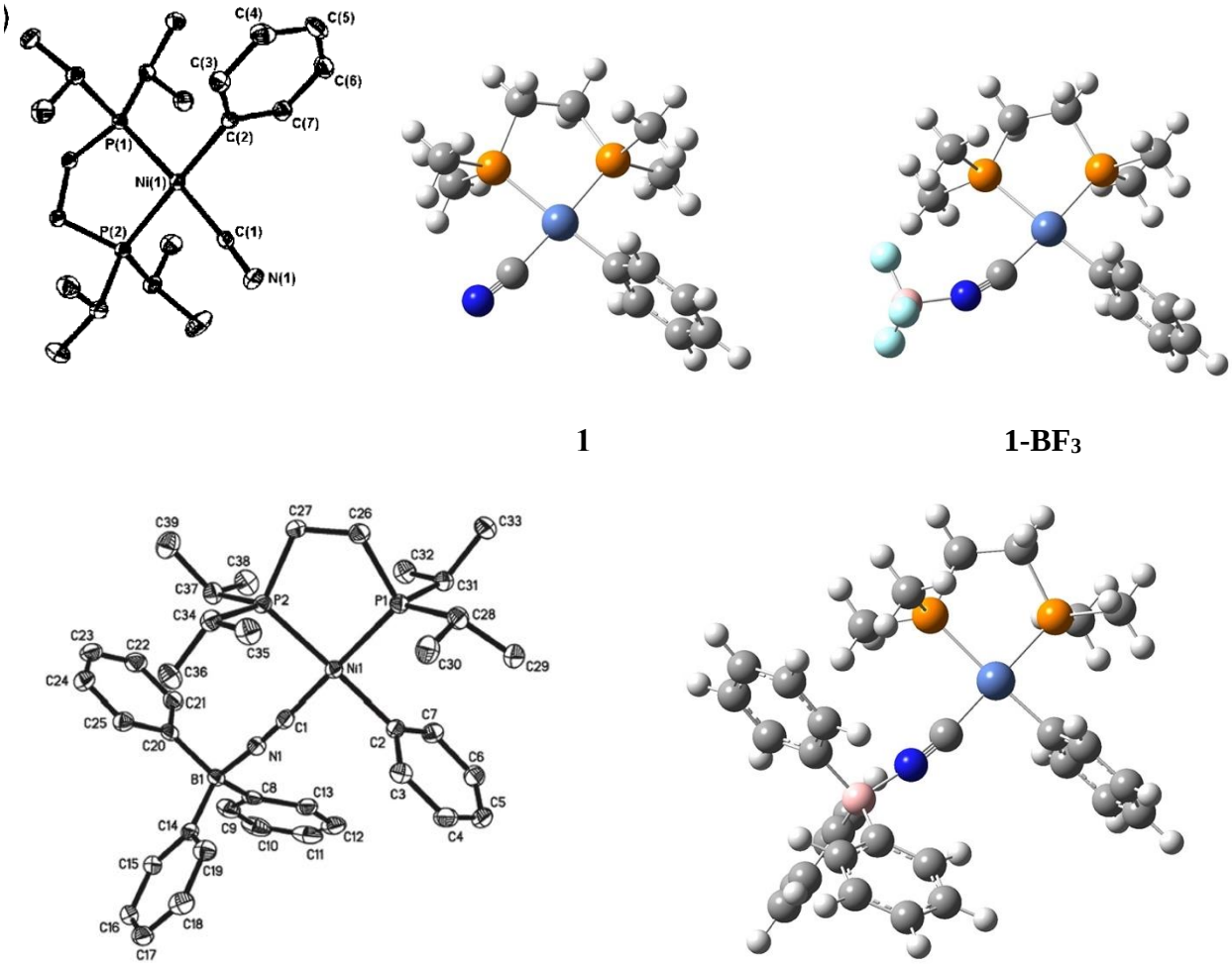

Figure 13: Comparison of the optimized and X-ray crystal structures of the C—CN bond activation product.

Table 3: Selected bond distances (Å) and angles (°) for the X-ray crystal structure and the optimized structure calculated by using Gaussian16, B3LYP/C, H, N, B, F (6-31G**), Ni, P (SDDALL) a_{Ni} = 3.130, a_P = 0.387) for the C—CN bond activation product.

	C–N	NI– CN	NI– C1	N–B	NI–N–C	C–NI–C	C–N–B
1	1.17139	1.86663	1.92499	-----	4.86333	92.17894	-----
1*	1.148(3)	1.877(3)	1.935(2)	-----	-----	89.62(10)	-----
1-BF_3	1.16375	1.85397	1.92680	1.62855	8.17	93.21	157.79
1-BPH_3	1.16341	1.85809	1.92814	1.58034	4.01	90.66	172.86

Table 3, cont.

1-BPH$_3$[*]	1.153(2)	1.8567(19)	1.9302(17)	1.575(2)	176.03(16)	89.13(7)	175.94(17)

[*]From the X-ray single crystal structures

The X-ray single crystal structures and optimized structures of the η^2 complexes are shown in **Figure 14** and selected bond distances (Å) and angles (°) are summarized in **Table 4**. The phenyl group is in the same plane as the CN group for both η^2-CN complex, **2**, and BF_3 coordinated η^2-CN complex, **2-BF$_3$**, with Ni-C-C1-C2 dihedral angle of 2.41 and -1.11, respectively. On the other hand, BPh_3 coordinated η^2-CN complex, **2-BPh$_3$**, has Ni-C-C1-C2 dihedral angle of -33.76 due to the steric bulk of BPh_3 and the phenyl group rotated. All the C—N bond distances are longer than the C, N triple bond. There are no notable deviations among the bond lengths. The average C—N bond lengths showed an average bond distance of 1.241 Å with a standard variation of ± 0.005 Å. The Ni—N bond lengths had an average value of 1.88 Å with the **2** being the longest and **2-BF$_3$** being the shortest bond length. The average length of the Ni—CN bonds is 1.87 Å. N—B bond length are almost the same for **2-BF$_3$** (1.59 Å) and **2-BPh$_3$** (1.60 Å). The Ni—N—B and C—N—B are both bent with around 140° and 150°, respectively.

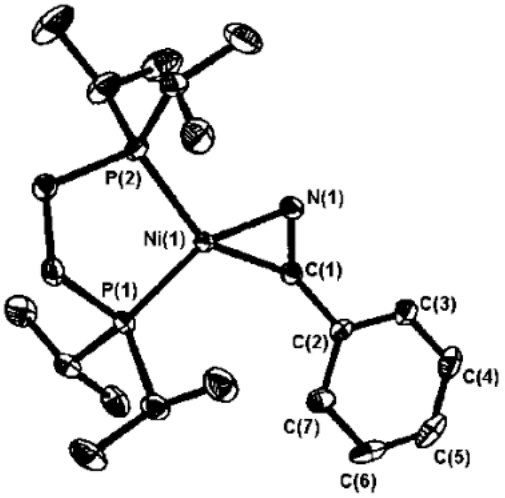
P(2)
N(1)
Ni(1)
C(1)
P(1)
C(3)
C(2)
C(4)
C(7)
C(5)
C(6)

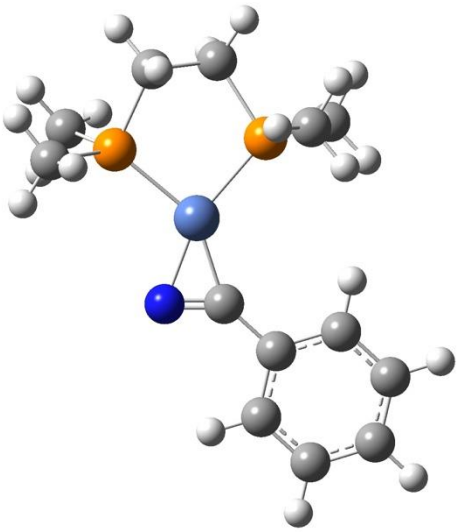

2

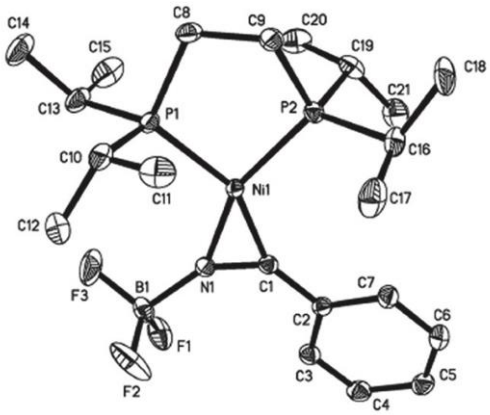
C14
C8
C9
C20
C15
C19
C18
C13
P1
P2
C21
C10
C16
C11
Ni1
C17
C12
F3
B1
N1
C1
C7
C2
C6
F1
C3
C5
F2
C4

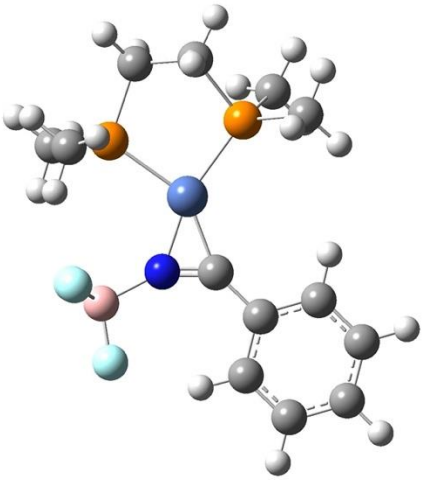

2-BF_3

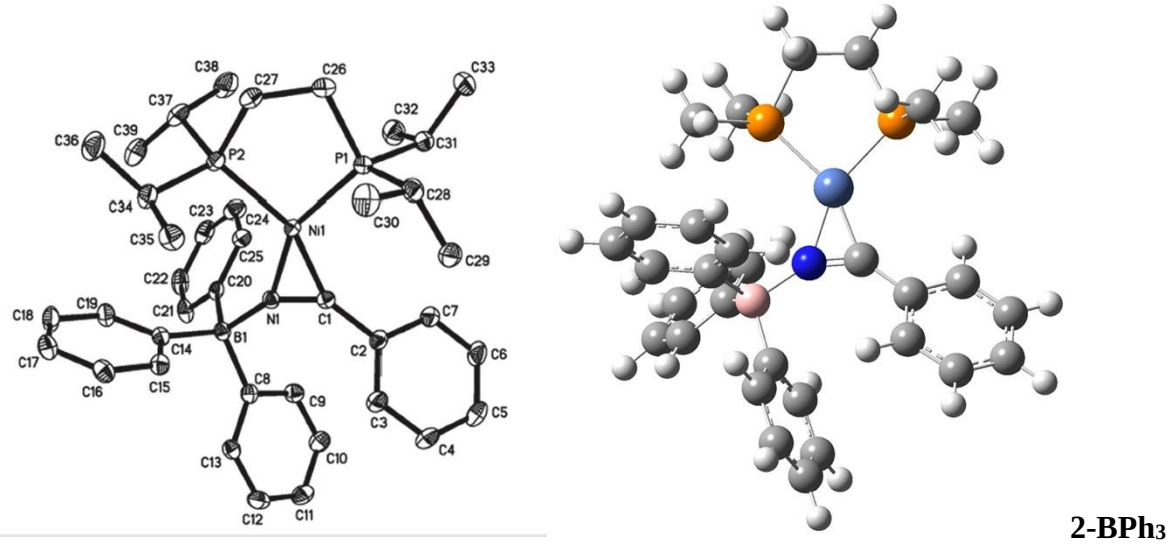

2-BPh3

Figure 14: Comparison of the optimized and X-ray crystal structures of the η^2-nitrile complex.

Table 4: Selected bond distances (Å) and angles (°) for the X-ray crystal structure and the optimized structure calculated by using Gaussian16, B3LYP/C, H, N, B, F (6-31G**), Ni, P (SDDALL) aNi = 3.130, aP = 0.387) for the h^2-nitrile complex.

	C–N	NI–N	NI– CN	N–B	B–N– NI	N–C–NI	C–N–B
2	1.23414	1.90140	1.87385	-----	-----	72.13	-----
2*	1.225(6)	1.908(3)	1.867(4)	-----	-----	-----	-----
2-BF_3	1.24465	1.83695	1.87607	1.59450	135.82	68.73	151.98
2-BF_3*	1.2524(19)	1.8684(13)	1.8499(15)	1.58(2)	146.19(11)	71.12(9)	144.19(14)
2-BPH_3	1.24185	1.89171	1.85583	1.60714	141.29	72.22	149.62
2-BPH_3*	1.241(2)	1.8866(14)	1.8542(17)	1.604(2)	146.1(12)	72.05(10)	143.37(15)

*From the X-ray single crystal structures

The optimized structures of the C—CN bond activation transition states are shown in **Figure 15** and selected bond distances (Å) and angles (°) are summarized in Table 5. The CN group is almost in the same plane as the P—Ni—P plane with the P—Ni—C—N dihedral angle of 5.9° in **TS12-BF_3**. On the other hand, CN group moved out of plane with the P—Ni—C—N dihedral angle of 28.5° in **TS12a** and -31.1° in **TS12b**. The C—N bond length is longer in **TS12-BF_3** (1.20 Å) compared to **TS12a** and **TS12b** (1.19 Å). The Ni—CN bond length is considerably shorter in **TS12-BF_3** (1.78 Å) compared to **TS12a** and **TS12b** (1.87 Å). The Ni—C_{aryl} bonds are similar within 2.03-2.04 Å. The C— C_{aryl} bond lengths is longer in **TS12-BF_3** (1.70 Å) compared **TS12a** and **TS12b** (1.59-1.60 Å). The C—N—B is still bent (135°) in the TS structure.

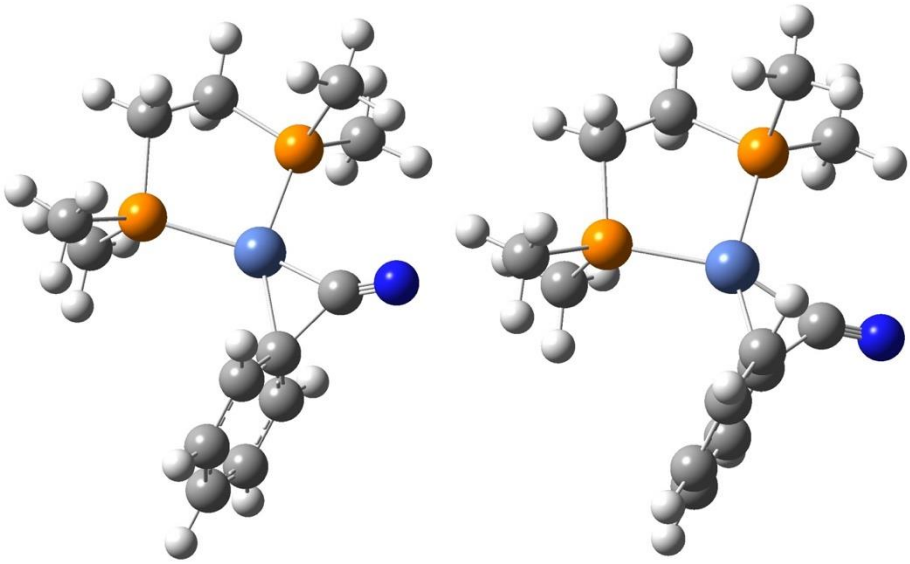

TS12a **TS12b**

TS12-BF_3

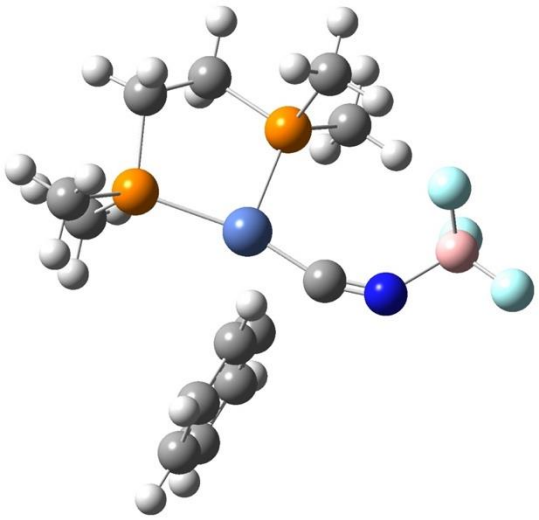

Figure 15: Comparison of the optimized C—CN bond activation TS structures with and without BF3.

Table 5: Selected bond distances (Å) and angles (°) for the optimized structures of C—CN bond activation TS structures with and without BF_3 calculated by using Gaussian16, B3LYP/C, H, N, B, F (6-31G**), Ni, P (SDDALL) a_{Ni} = 3.130, a_P = 0.387)

	C–N	NI– CN	NI– C1	N–B	C1–C	NI–N–C	C–NI–C	C–N–B
TS12A	1.18928	1.86852	2.02660	-----	1.60209	19.56	48.36	-----
TS12B	1.18946	1.87531	2.03514	-----	1.58759	20.21	47.69	-----
TS12-BF_3	1.19832	1.78498	2.03632	1.60764	1.69910	12.50	52.30	134.65

Future work

From the TS structures located on the PES of the C—CN bond activation with and without the Lewis acid coordination, our research group will follow the reaction coordinate with the intrinsic reaction coordinate calculations and complete the reaction profile. The main challenge is to study the post-transition bifurcation following the Lewis acid assisted C—CN bond activation TS. The initial difficulties in locating the TS structures with the added Lewis acid is due to the considerable changes on the PES. We will also take into consideration solvent effects in future DFT calculations using SMD.

CHAPTER V

Conclusion

The first attempt of finding the TS structure for the C—CN bond activation of benzonitrile with the [Ni(dmpe)] fragment in the presence of a Lewis acid (BF_3) by simply adding BF_3 to already located TS structures without BF_3 failed. Therefore, the potential energy surface was further investigated in the presence of a Lewis acid (BF_3) via 1D and 2D scans and compared with the scans without BF_3. The X-ray single crystal structures of the C—CN bond activation products were used as a starting geometry. These scans gave only one distinct TS structure with BF_3. There are two distinct TS structures without BF_3. Selected bond distances (Å) and angles (°) of the optimized structures for the η^2-nitrile complexes and the C—CN bond activation products show excellent agreement with the X-ray single crystal structures. The C— CN bond length for the TS structure with BF_3 (1.70 Å) is longer than the TS structures without BF_3 (1.59-1.60 Å). The nitrile group is almost in the same plane as the P—Ni—P plane in the TS structure with BF_3, whereas it is out of plane in the TS structures without BF_3. In future work, these TS structures will be followed to complete the reaction profile. Solvent effects will also be considered in future DFT calculations using SMD, due to the high polarity of the C—CN bond activation products.

REFERENCES

Acosta-Ramírez, A., Muñoz-Hernández, M., Jones, W. D., & García, J. J. (2007). Catalytic isomerization of 2-methyl-3-butenenitrile by nickel systems using bis-diphosphinoferrocene ligands: Evidence for hemilability. *Organometallics*, *26*(24), 5766–5769. https://doi.org/10.1021/om700928y

Amusia, M. Y., Msezane, A. Z., & Shaginyan, V. R. (2003). Density Functional Theory versus the Hartree–Fock Method: Comparative Assessment. *Physica Scripta*, *68*(6), C133–C140. https://doi.org/10.1238/physica.regular.068ac0133

Becke, A. D. (1993). Density-functional thermochemistry. III. The role of exact exchange. *The Journal of Chemical Physics*, *98*(7), 5648–5652. https://doi.org/10.1063/1.464913

Becke, A. D. (2014). Perspective: Fifty years of density-functional theory in chemical physics. *Journal of Chemical Physics*, *140*(18). https://doi.org/10.1063/1.4869598

Brunkan, N. M., Brestensky, D. M., & Jones, W. D. (2004). Kinetics, Thermodynamics, and Effect of BPh3 on Competitive C-C and C-H Bond Activation Reactions in the Interconversion of Allyl Cyanide by [Ni(dippe)]. *Journal of the American Chemical Society*, *126*(11), 3627–3641. https://doi.org/10.1021/ja037002e

Clot, E., Besora, M., Maseras, F., Mégret, C., Eisenstein, O., Oelckers, B., & Perutz, R. N. (2003). Bond energy M-C/H-C correlations: Dual theoretical and experimental approach to the

sensitivity of M-C bond strength to substituents. *Chemical Communications*, *3*(4), 490–491. https://doi.org/10.1039/b210036n

Crabtree, R. H., Holt, E. M., Lavin, M., & Morehouse, S. M. (1985). Inter- vs. intramolecular carbon-hydrogen activation: a carbon-hydrogen-iridium bridge in [IrH2(mq)L2]BF4 and a CH + M .fwdarw. CMH reaction trajectory. *Inorganic Chemistry*, *24*(13), 1986–1992. https://doi.org/10.1021/ic00207a008

Ehlers, A. W., Böhme, M., Dapprich, S., Gobbi, A., Höllwarth, A., Jonas, V., Köhler, K. F., Stegmann, R., Veldkamp, A., & Frenking, G. (1993). A set of f-polarization functions for pseudo-potential basis sets of the transition metals ScCu, YAg and LaAu. *Chemical Physics Letters*, *208*(1–2), 111–114. https://doi.org/10.1016/0009-2614(93)80086-5

Forlemu, N., Watkins, P., & Sloop, J. (2017). Molecular Docking of Selective Binding Affinity of Sulfonamide Derivatives as Potential Antimalarial Agents Targeting the Glycolytic Enzymes: GAPDH, Aldolase and TPI. *Open Journal of Biophysics*, *07*(01), 41–57. https://doi.org/10.4236/ojbiphy.2017.71004

García, J. J., Arévalo, A., Brunkan, N. M., & Jones, W. D. (2004). Cleavage of carbon-carbon bonds in alkyl cyanides using nickel(0). *Organometallics*, *23*(16), 3997–4002. https://doi.org/10.1021/om049700t

Garcia, J. J., Brunkan, N. M., & Jones, W. D. (2002). Cleavage of carbon-carbon bonds in aromatic nitriles using nickel(0). *Journal of the American Chemical Society*, *124*(32), 9547–9555.

https://doi.org/10.1021/ja0204933

Hehre, W. J., Ditchfield, K., & Pople, J. A. (1972). Self-consistent molecular orbital methods. XII. Further extensions of gaussian-type basis sets for use in molecular orbital studies of organic molecules. *The Journal of Chemical Physics*, *56*(5), 2257–2261. https://doi.org/10.1063/1.1677527

Höllwarth, A., Böhme, M., Dapprich, S., Ehlers, A. W., Gobbi, A., Jonas, V., Köhler, K. F., Stegmann, R., Veldkamp, A., & Frenking, G. (1993). A set of d-polarization functions for pseudo-potential basis sets of the main group elements AlBi and f-type polarization functions for Zn, Cd, Hg. *Chemical Physics Letters*, *208*(3–4), 237–240. https://doi.org/10.1016/0009-2614(93)89068-S

Hopmann, K. H. (2016). How accurate is DFT for iridium-mediated chemistry? *Organometallics*, *35*(22), 3795–3807. https://doi.org/10.1021/acs.organomet.6b00377

Hugo, V.-V. V., Alejandro, H.-S. M., María, V.-S. A., María, R.-H., Antonio, L.-R. M., Guadalupe, P.-O. M., Antonio, M.-G. M., Fernando, A.-H., Víctor, A., Diego, C.-A., & Enrique, Á. (2019). Molecular Modeling and Synthesis of Ethyl Benzyl Carbamates as Possible Ixodicide Activity. *Computational Chemistry*, *07*(01), 1–26. https://doi.org/10.4236/cc.2019.71001

Krishnan, R., Binkley, J. S., Seeger, R., & Pople, J. A. (1980). Self-consistent molecular orbital methods. XX. A basis set for correlated wave functions. *The Journal of Chemical Physics*,

72(1), 650–654. https://doi.org/10.1063/1.438955

Laird, B. B., Ross, R. B., & Ziegler, T. (1996). *Density-Functional Methods in Chemistry : An Overview Density-functional theory (DFT), in its various forms , has become an important research tool for chemists , physicists and materials scientists . Its development in recent years has proceeded along* . 1–17.

Lecklider, T. (2011). Maintainng a heathy rhythm. *EE: Evaluation Engineering*, *50*(11), 36–39.

Li, K., & Xue, D. (2006). Estimation of electronegativity values of elements in different valence states. *Journal of Physical Chemistry A*, *110*(39), 11332–11337. https://doi.org/10.1021/jp062886k

Li, T., García, J. J., Brennessel, W. W., & Jones, W. D. (2010). C-CN bond activation of aromatic nitriles and fluxionality of the η2-arene intermediates: Experimental and theoretical investigations. *Organometallics*, *29*(11), 2430–2445. https://doi.org/10.1021/om100001m

Lundberg, M., & Siegbahn, P. E. M. (2005). Quantifying the effects of the self-interaction error in DFT: When do the delocalized states appear? *Journal of Chemical Physics*, *122*(22). https://doi.org/10.1063/1.1926277

Marenich, A. V., Cramer, C. J., & Truhlar, D. G. (2009). Universal solvation model based on solute electron density and on a continuum model of the solvent defined by the bulk dielectric constant and atomic surface tensions. *Journal of Physical Chemistry B*, *113*(18), 6378–6396. https://doi.org/10.1021/jp810292n

Martin, R., & Buchwald, S. L. (2008). Palladium-catalyzed suzuki-miyaura cross-coupling reactions employing dialkylbiaryl phosphine ligands. *Accounts of Chemical Research*, *41*(11), 1461–1473. https://doi.org/10.1021/ar800036s

Martinez, J. L., Lin, H. J., Lee, W. T., Pink, M., Chen, C. H., Gao, X., Dickie, D. A., & Smith, J. M. (2017). Cyanide Ligand Assembly by Carbon Atom Transfer to an Iron Nitride. *Journal of the American Chemical Society*, *139*(40), 14037–14040. https://doi.org/10.1021/jacs.7b08704

Munjanja, L., Torres-López, C., Brennessel, W. W., & Jones, W. D. (2016). C-CN Bond Cleavage Using Palladium Supported by a Dippe Ligand. *Organometallics*, *35*(11), 2010–2013. https://doi.org/10.1021/acs.organomet.6b00304

Nakao, Y., Hirata, Y., & Hiyama, T. (2006). Cyanoesterification of 1,2-dienes: Synthesis and transformations of highly functionalized α-cyanomethylacrylate esters. *Journal of the American Chemical Society*, *128*(23), 7420–7421. https://doi.org/10.1021/ja0606834

Nakazawa, H., Kamata, K., & Itazaki, M. (2005). Catalytic C-C bond cleavage and C-Si bond formation in the reaction of RCN with Et3SiH promoted by an iron complex. *Chemical Communications*, *31*, 4004–4006. https://doi.org/10.1039/b504131g

Peng, C., Ayala, P. Y., Schlegel, H. B., & Frisch, M. J. (1996). to Optimize Equilibrium Geometries and Transition States. *Journal of Computational Chemistry*, *17*(1), 49–56.

Pettersen, E. F., Goddard, T. D., Huang, C. C., Couch, G. S., Greenblatt, D. M., Meng, E. C., &

Ferrin, T. E. (2004). UCSF Chimera - A visualization system for exploratory research and analysis. *Journal of Computational Chemistry*, *25*(13), 1605–1612. https://doi.org/10.1002/jcc.20084

Peverati, R., & Truhlar, D. G. (2012). M11-L: A local density functional that provides improved accuracy for electronic structure calculations in chemistry and physics. *Journal of Physical Chemistry Letters*, *3*(1), 117–124. https://doi.org/10.1021/jz201525m

Properties, T. C., Complexes, L. M., Work, E., Containing, C., Complexes, A., Considerations, T., Activation, A., Additlon, O., Activation, A., Systems, O., Considerations, K., Breaking, B., Alkanes, S., Breaking, B., Alkanes, U., Activation, A., Surfaces, M., Homogeneity, C., Reactions, A., … Activation, A. (1985). *The Organometallic Chemistry of Alkanes*.

Souillart, L., & Cramer, N. (2015). Catalytic C-C Bond Activations via Oxidative Addition to Transition Metals. *Chemical Reviews*, *115*(17), 9410–9464. https://doi.org/10.1021/acs.chemrev.5b00138

Swartz, B. D., Brennessel, W. W., & Jones, W. D. (2011). C-CN vs C-H cleavage of benzonitrile using [(dippe)PtH]2. *Organometallics*, *30*(6), 1523–1529. https://doi.org/10.1021/om101069j

Taw, F. L., White, P. S., Bergman, R. G., & Brookhart, M. (2002). Carbon-carbon bond activation of R-CN (R = ME, Ar, iPr, tBu) using a cationic Rh(III) complex. *Journal of the American Chemical Society*, *124*(16), 4192–4193. https://doi.org/10.1021/ja0255094

Yu, H. S., Li, S. L., & Truhlar, D. G. (2016). Perspective: Kohn-Sham density functional theory descending a staircase. *Journal of Chemical Physics*, *145*(13). https://doi.org/10.1063/1.4963168

Zhao, Y., Ng, H. T., Peverati, R., & Truhlar, D. G. (2012). Benchmark database for ylidic bond dissociation energies and its use for assessments of electronic structure methods. *Journal of Chemical Theory and Computation*, *8*(8), 2824–2834. https://doi.org/10.1021/ct300457c

BIOGRAPHICAL SKETCH

Lubna Kader was born in Bangladesh on January 12th, 1994. While growing up, she always had a fondness for science. She attended the University of Rajshahi, Bangladesh, from where she received a Bachelor of Science and Master of Engineering in Applied Chemistry and Chemical Engineering. She started her master's program in Chemistry at University of Texas Rio Grande Valley in the year of 2021. Throughout her Master's program, Lubna served the Chemistry department of UTRGV as a Graduated Research Assistant and Graduate Teaching Assistant in different academic semesters. During this working period, she learned a lot of things including teach a multitude of courses and laboratories work of different academic courses such as General Chemistry, Organic Chemistry and Biochemistry. Finally, she graduated with her master's in chemistry from UTRGV on December 16th , 2022.

Permanent Mailing Address: 3003 Rolling Fog Drive, Friendswood, TX 77546, USA.

Author can be reached at : lubnak66@gmail.com